Photographic evidence for the third-order rainbow

Michael Großmann,[1] Elmar Schmidt,[2] and Alexander Haußmann[3,*]

[1]Arbeitskreis Meteore e.V., Große Brunnenstr. 18, D-75236 Kämpfelbach, Germany

[2]SRH University of Applied Sciences, Bonhoefferstr. 11, D-69123 Heidelberg, Germany

[3]Institute of Applied Photophysics, Technische Universität Dresden,
George-Bähr-Str. 1, D-01069 Dresden, Germany

*Corresponding author: haussmann@iapp.de

The first likely photographic observation of the tertiary rainbow caused by sunlight in the open air is reported and analyzed. Whereas primary and secondary rainbows are rather common and easily seen phenomena in atmospheric optics, the tertiary rainbow appears in the sunward side of the sky and is thus largely masked by forward scattered light. Up to now, only a few visual reports and no reliable photographs of the tertiary rainbow are known. Evidence of a third-order rainbow has been obtained by using image processing techniques on a digital photograph that contains no obvious indication of such a rainbow. To rule out any misinterpretation of artifacts, we carefully calibrated the image in order to compare the observed bow's angular position and dispersion with those predicted by theory. © 2011 Optical Society of America

OCIS codes: 010.1290, 010.1310, 010.3920, 010.7295.

1. Introduction

The rainbow has always been the best-known phenomenon in atmospheric optics, and has moreover triggered much research in the field of theoretical physics from the early stages of this discipline until today. Many optical theories have been used to explain the rainbow, culminating in the 20th century's complex theories for the scattering of light by dielectric spheres [1]. Not all these theoretical predictions are visible in a natural rainbow display due to the Sun's finite angular diameter, its broad spectral emittance, and the natural mixture of drop sizes in a typical rain shower [2]. Accordingly, in most natural rainbows one will only see the bright primary and the weaker secondary bow, and sometimes several supernumerary bows inside the primary [3]. The latter are due to interference between the wave fronts causing the primary rainbow, but still are sometimes erroneously described as "third," "fourth," etc. rainbows.

In recent years, the proliferation of unusual rainbow photographs by amateur observers has added unexpected features to these basic ones, e.g., twinned and kinked rainbows [4,5] or reflection rainbows extending up into the sky [6]. However, all the anomalies mentioned before are unrelated to the much more fundamental question within the community of rainbow enthusiasts of why tertiary (third-order) rainbows or even higher-order bows are usually not seen in nature [7].

Part of the answer is given by the intensity reduction during each reflection (with none of them being total) and the increasing angular dispersion, i.e., the radial width of the bows. Already, the secondary rainbow appears much weaker than the primary, and seldom has a substantial contrast with respect to the background. However, much more important is the fact that both the tertiary and quaternary bow appear in the sunward side of the sky at angular distances of 37°–49° from the Sun according to geometric optics (as can be calculated by Eqs. (1.3) and (1.6) from [8]). Within this celestial region, an intense background illumination arises from external reflection at the water drop surface and, more prominently,

transmission without internal reflections occurs within the drop. The ensuing disk of light centered on the Sun is therefore commonly referred to as "zero-order glow" [9] and adds intensity to the other mechanisms of forward scattering of sunlight by aerosol. Both geometric optics and the exact electro-dynamic solution (Mie theory) predict an almost total loss of contrast for these rainbows [10]. Figure 1 shows the angle dependent scattering efficiency of a spherical water drop according to geometric optics up to the rainbow of fifth order. As seen, the tertiary rainbow is masked by an approximately 10 times brighter zero-order glow [11]. More advanced theories such as the Debye series give even lower contrast values in the range of $1/40 - 1/17$ for drop sizes in the range of 0.1–1 mm [12].

Despite these problems, or rather because of these challenges, the search for the tertiary rainbow has intrigued many observers over three centuries since its position was first predicted by Edmond Halley, who had also calculated the correct position for the quaternary rainbow [13]. In addition to coping with the exceedingly low contrast as stated above, persons unfamiliar with atmospheric optics may confuse the enigmatic tertiary rainbow with ice-crystal halos of the 46° radius family, which can become much brighter. In at least one prominently documented 19th-century case, the claim of a tertiary rainbow sighting [14] had to be withdrawn as actually being a halo. A compilation of odd phenomena in atmospheric optics leaves open the reality of tertiary rainbows in the outdoors, although many colored phenomena in the sky were wrongly called "rainbows", e.g., early sightings of the circumhorizon arc as "horizontal rainbows" [15].

A list of more credible reports of a tertiary rainbow is given in [16], the last of which is from Nairobi,

Kenya [17]. Before the spring of 2011, we know of no reliable photographs of the natural tertiary rainbow.

Nonetheless, higher-order bows have made their way into scientific labs as in the classic experiment of Walker, who was able to record the first 13 rainbows from a single drop under white light and Helium-Neon laser illumination [18], and its historic predecessors cited therein, tracking back to the earliest work of Billet from the 19th century [19].

2. Observational and Photographical Details

Recent interest in the tertiary bow was triggered by talks of Raymond L. Lee and Philip Laven, who examined the chances for observing it in nature from a theoretical point of view at the 10th Light and Color in Nature Meeting at St. Mary's College of Maryland in June 2010. These talks were later condensed into a joint article [20]. Within the German amateur observers' network "Arbeitskreis Meteore e.V. (AKM)" [21], several observers took up the challenge and prepared to obtain the first reliable photograph of the tertiary rainbow. Since the phenomenon is unlikely to be seen by the unaided human eye, this often means taking photographs "blindly" in the right direction.

In the evening of May 15, 2011, one of the authors (M. Großmann) noticed a rain shower approaching from the north at his home in Kämpfelbach in southwestern Germany. After reaching his preferred observation site (48°56.5′N, 8°36.7′E), both primary and secondary rainbows were already visible. Rain at his position then intensified, offering the chance for a tertiary bow as sunlit drops were now located in the correct angular positions. Furthermore, on the left side of the Sun a relatively dark cloud bank drastically reduced the background illumination. With the Sun blocked by a tree, he could see no definite rainbow pattern, only a faint trace of it at the limit of visibility for about 30 seconds. This visual sensation was of a shimmering nature, thus possibly involving glints of light or color obtained from individual drops in the sunward sheets of heavy rain [22,23]. A similar impression has been reported before as "scintillating" [24].

The digital photographic camera (Canon EOS 450D, equipped with an EF-S 18–55 mm lens, zoom position at $f = 18$ mm) was placed in a box in order to protect it from the intense rain, because, in an earlier attempt, raindrops on the lens produced circular, albeit not Sun-centered image artifacts. Photographs were taken in RAW mode to prevent any compression artifacts. All additional processing functions of the camera were deactivated. None of the images showed the tertiary rainbow when first inspected but, after unsharp masking and contrast enhancement, a colored, bow-like pattern with a red rim at the outside was clearly visible in one picture (taken at 18:00 UTC). Figure 2 shows both the unprocessed and the enhanced version of this image.
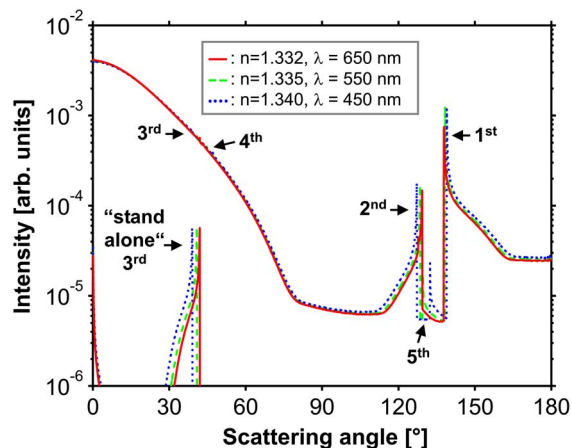

Fig. 1. (Color online) Distribution of the scattered intensity per solid angle from a water sphere in air as function of the scattering angle, according to geometric optics. Within this ray tracing calculation, up to five internal reflections are considered. The calculation has been done for three different wavelengths and both polarizations have been summed up. Numbers indicate the rainbow order. For comparison, the contribution from the tertiary rainbow is included.
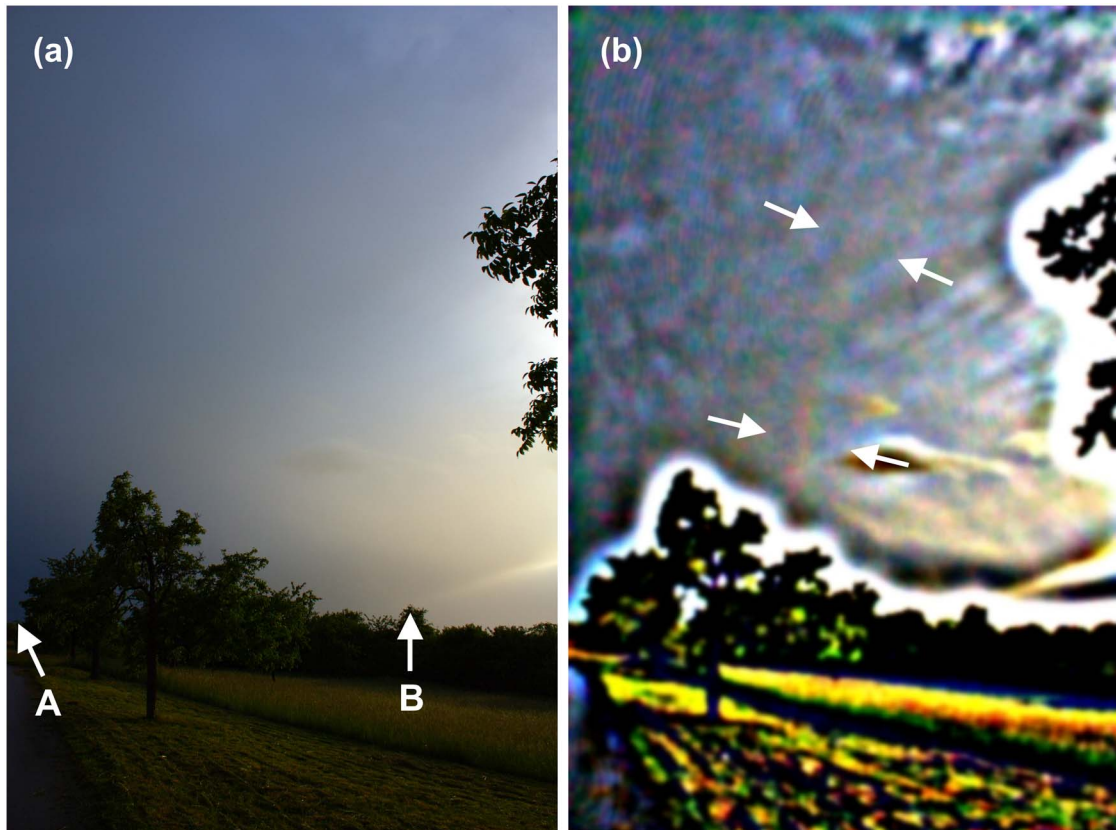
Fig. 2. (Color online) (a) Original image from May 15, 2011, 18:00 UTC, Kämpfelbach, Germany. Two reference positions (A and B) for image orientation are indicated. (b) Processed version after contrast expansion and unsharp masking, showing a rainbow like pattern next to the image center, marked by the arrows. The solar elevation is 8.1°. Our analysis (Section 3.A) shows that the center of the picture points to 18.7° elevation and 252.1° azimuth, with an anticlockwise rotation angle of the image with respect to the vertical of 2.6°.

3. Image calibration and Analysis

A. Calibration and Orientation

In order to prove that the colored circular pattern in the photo is indeed the tertiary rainbow, a careful analysis of the angular distance from the Sun was carried out by means of standard spherical geometry. Since both position and time of the photograph are known, the calculation of the Sun's position is easy and gives 8.1° elevation and 289.6° azimuth, both to an accuracy of 0.1° due to the remaining uncertainties of time calibration. The main task is to reconstruct celestial coordinates for the individual pixels of the photograph, in order to assign them a well-defined angular distance from the Sun. To do so, a star field image was taken with the same camera and the lens at the same zoom level. By this, it is possible to determine the relation between the field angle ϑ (angular distance of an object from the optical axis) and the distance R from the image center, measured in the unit of a single pixel width. To do so, a second-order polynomial was fitted to the data obtained for ~20 stars. At the original image resolution, this results in the equation:

$$R = 3633.7 \tan \vartheta - 262.45 \tan^2 \vartheta. \qquad (1)$$

Note that the first-order coefficient of Eq. (1) corresponds to a focal length of 18.9 mm, to be calculated from the sensor size of 14.8 mm × 22.2 mm and the full image resolution of 2848 × 4272 pixels. The second-order term represents a certain amount of barrel distortion, as is common for wide-angle zoom lenses.

Still left to determine are the three angles defining the camera's orientation, namely the elevation and azimuth of the optical axis and the rotation of the sensor around this axis. The value of the last parameter will be small, since usually the photographer will try to keep the horizon as a horizontal line in the image. Nonetheless, it cannot be neglected in order to achieve the necessary degree of accuracy in the analysis. All three angles can be calculated from only two reference points in the picture with known elevation and azimuth by adapting routines of standard spherical geometry [25,26]. Preferably, these will be stars or planets (as possible for photographs of noctilucent clouds or lunar ice-crystal halos [27]). However, in our case, landmarks such as trees had to be chosen since they are the only reasonably fixed features in both the rainbow and the star field image.

We solved the problem by choosing two rather distant treetops or branches as references and calculated their unknown celestial coordinates from a star

field picture, which was taken on June 02, 2011 at 21:22 UTC as close as possible to the position of the tertiary bow photograph [see Fig. 2(a) and 3]. With this technique, parallax effects will be minimized. The three crucial angles for the star field image were previously calculated from two stars. The results for this indirect method of registering the daylight with the night-time image are given in the caption to Fig. 2. The estimated error margin for the given values is about 0.2°, resulting from the limited time calibration accuracy for the star field image and the remaining parallax error.

It should be noted that we used one and the same star field image (Fig. 3) to serve the two different purposes of determining the lens calibration Eq. (1) and reconstructing both elevation and azimuth of the reference positions A and B in Fig. 2(a).

B. Rainbow Analysis

For our analysis, three methods have been employed: (1) Defining sample points at the bow with subsequent calculation of their distance from the Sun, (2) plotting circles corresponding to the Descartes angles into the image for visual comparison, and (3) quantitative readout of brightness data from the image file with subsequent averaging over the clock angle (i.e., the azimuth within the Sun-centered coordinate system) for given angular distances from the Sun.
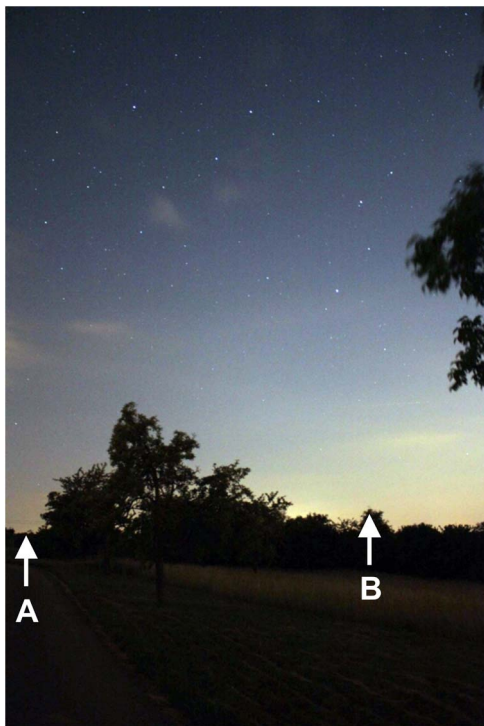

Fig. 3.   (Color online) Star field image used for calibration of the rainbow image. Elevation and azimuth of the positions A and B can be calculated using stars as references. These positions can be identified in the original image [Fig. 2(a)], taken from approximately the same position, thus serving as references to locate the recorded bow at the celestial sphere (picture taken on June 02, 2011, 21:22 UTC).

To carry out the first method, several points at the outermost red boundary of the bow were selected and localized in the processed and tenfold downsized version (285 × 428 pixel) of the original image [see Fig. 4(a)]. The origin of the x and y pixel coordinates is the image center. The results are given in Table 1. They fit well the theoretical expectation of 41.5° ($\lambda = 600$ nm) angular distance from the Sun for red light. The remaining difference of 0.2–0.4° is mostly accounted for by the uncertainties in both the Sun's position and the image's orientation, but it might also be attributed to unknown details of the CMOS red sensor's spectral response, drop-size dependent deviations from geometric optics, the finite diameter of the Sun, or shifts of the bow position due to the strong image processing.

We now address some restrictions of using a commercial digital camera for this work. For color image generation, the intensities for each of three color sensors in a group of camera pixels are projected into a color space like sRGB by usually hidden algorithms. As we used the camera's raw data for this work we must address the spectral characteristics of the red, green, and blue sensors, for which only coarse and diagrammatic information was found [28]. Because of the quite asymmetric shape of each sensor's spectral profiles there is a sizeable difference between their peak and centroid (i.e., mean) wavelengths, which we calculated for the three sensors (see Table 2).

In the case of the extremely low contrast tertiary rainbow photograph, we think that the peak sensitivity of each sensor largely determines the rainbow's exact pixel position. To include the reddening effect in the evening sunlight we further increased these values by dominant wavelength shifts, obtained by a combination of own calculations, and published data [29]. After rounding off the combined effects, we arrived at the wavelengths of choice given in the fifth column of Table 2 as the basis for our comparisons with the tertiary rainbow's theoretical positions. In any case, it is clear that the spectral width of the primary colors as given by the camera sensors is quite reduced, spanning a range of only 140 nm from red to blue.

The refractive index of water is calculated according to [30], followed by a correction for the air environment ($n_{\text{Air}} = 1.00029$). By this, we obtained Descartes angles of 41.5° (red, 600 nm), 40.6° (green, 530 nm), and 39.3° (blue, 460 nm) with respect to the Sun (see Table 2) [31].

The second way to visualize the correspondence between the imaged arc and the theoretical tertiary rainbow position requires the calculation of pixel coordinates for circles of equal angular distance from the Sun in the correct projection of the image. The results for the previously mentioned Descartes angles are shown in Fig. 4(b), with the small amount of barrel distortion of the lens included in the plotted circles. It should be noted that the position of a certain color within a real rainbow generated by
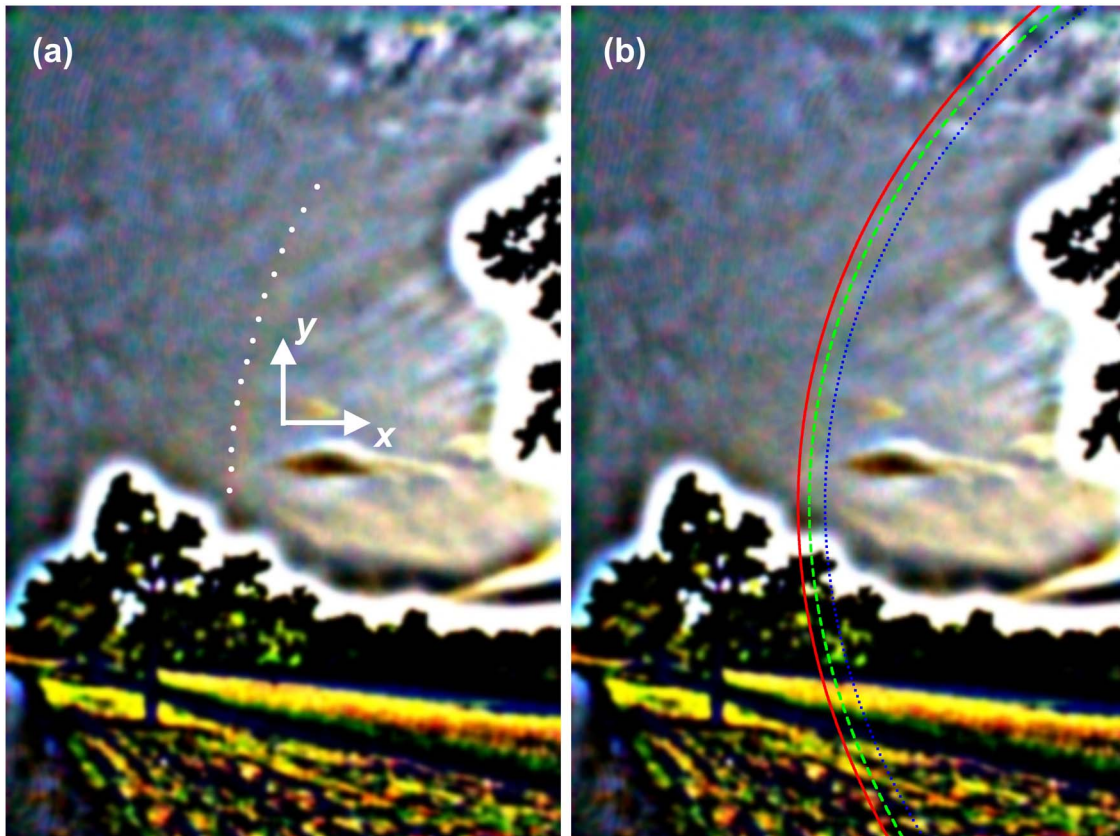
Fig. 4. (Color online) (a) Sample points (white circles) at the outermost red rim of the recorded bow. The x, y coordinate system for the determination of pixel coordinates of these sample points is indicated by white arrows. (b) Lines of equal angular distance from the Sun: 41.5° (red, solid), 40.6° (green, dashed), 39.3° (blue, dotted), corresponding to the Descartes angles for 600 nm, 530 nm, and 460 nm. Comparison with Fig. 2(b) reveals the coincidence of these circles with the rainbow.

sunlight does not necessarily have to coincide with its corresponding monochromatic scattering maximum and that this maximum itself will deviate from the Descartes angle depending on the drop size.

Table 1. Pixel Coordinates, Celestial Coordinates and Solar Distance for the Sample Points from Fig. 4(a)[a]

x [pixel]	y [pixel]	Elevation [°]	Azimuth [°]	Angular Distance from Sun [°]
17.5	121	37.3	256.5	41.8
10.5	109	35.6	255.1	41.8
4.5	99	34.1	253.8	41.9
−0.5	88	32.5	252.8	41.9
−4.5	75	30.6	251.9	41.8
−9.5	65	29.0	251.0	41.9
−12.5	53	27.1	250.3	41.7
−15.5	42	25.4	249.8	41.7
−18.5	31	23.7	249.2	41.7
−21.5	21	22.1	248.6	41.8
−23.5	10	20.4	248.2	41.8
−25.5	−3	18.3	247.9	41.8
−26.5	−14	16.6	247.7	41.8
−26.5	−24	15.0	247.6	41.7
−27.5	−35	13.3	247.4	41.8

[a]Note that the pixel coordinates were taken from a tenfold downsized version of the original image. The origin is the image center.

However, the matching of the recorded bow with the Descartes angles for red, green, and blue appears very satisfying in our view. This applies not only to the position, but furthermore to the angular width due to dispersion, as shown by the distance of the three plotted circles in Fig. 4(b).

Finally, a quantitative readout of brightness data from the unprocessed image at original resolution was carried out. These data were averaged over a clock angle segment of 40° from 29° to 59° solar distance (Fig. 5). The results are shown in Fig. 6(a). As expected, the intensity steps of the bow are barely visible. This corresponds to the barely discernible visual impression of the natural phenomenon as well as to the unprocessed image and matches the theoretical prediction of effective contrast loss due to the zero-order glow (Fig. 1).

Therefore, in order to extract the bow signal, a background subtraction was performed. The background characteristics for the individual color channels were determined by fitting a polynomial of degree four to the regions apart from the bow. As a result, the bow signal is clearly visible in each channel, being shifted according to the dispersion between the individual colors. The Descartes angles for red (600 nm), green (530 nm), and blue (460 nm) as marked by the vertical lines match the

corresponding intensity maxima quite well. The remaining small inward shift of each color maximum with respect to its extreme angle may be attributed to the uncertainties mentioned above (CMOS sensor response details, finite diameter of the Sun, position shifts due to image processing, image calibration, solar position) but may also indicate the limitations of geometrical optics.

Within Airy theory, such shifts of the main intensity maximum with respect to the Descartes angle are a familiar feature and increase with decreasing drop size. In the case of the tertiary bow, the shift is predicted to occur in a sunward direction, matching qualitatively our experimental data. However, since Airy theory only describes the neighborhood of a single caustic without any zero-order glow contribution, a quantitative simulation could only be compared to such background corrected data. In order to simulate the whole natural appearance of the phenomenon, the zero-order glow intensity would have to be added artificially while paying attention to the intensity balance between background and tertiary bow.

Consequently, when considering an upgrade of the theoretical description, Mie theory or the Debye series are the methods of choice [32] to overcome the limitations of geometric optics. Using the Debye series for a drop radius of about 1 mm, the peak intensities for the tertiary rainbow ($p = 4$) are found at 41.0° ($\lambda = 600$ nm), 40.2° ($\lambda = 530$ nm), and 38.9° ($\lambda = 460$ nm). This corresponds to an angular shift
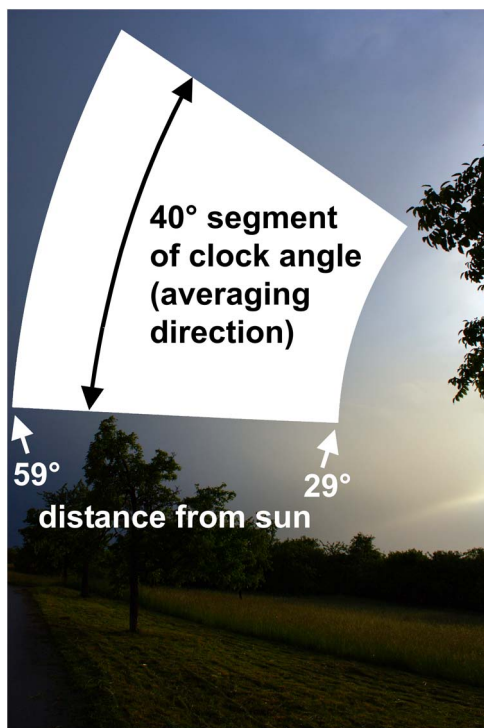

Fig. 5. (Color online) Sector area (white) for quantitative analysis of intensity, covering solar distances from 29° to 59° along a 40° section of the clock angle.
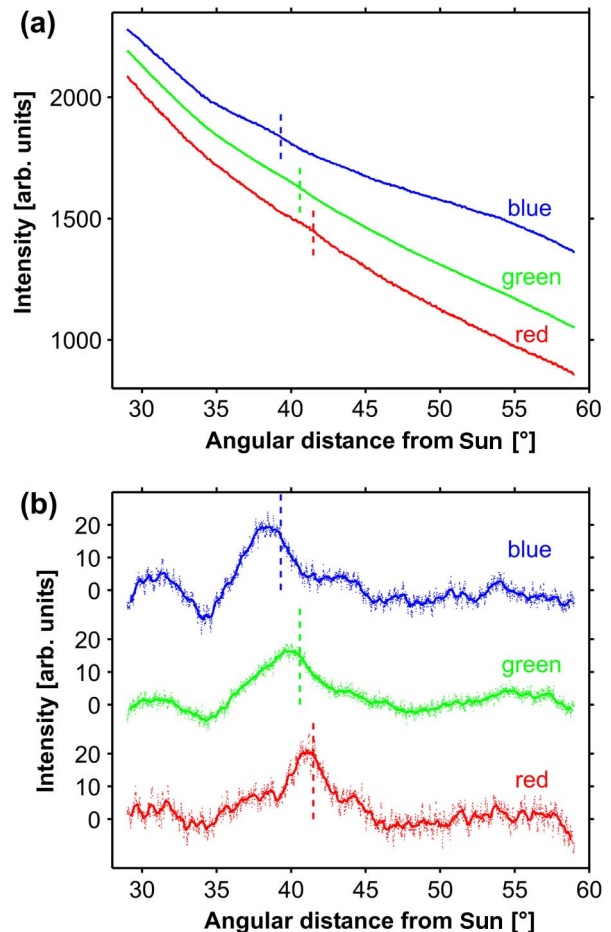

Fig. 6. (Color online) Brightness data of the red, green, and blue channel from the arc segment area marked in Fig. 5 as taken (a) from the original image and (b) after subtraction of an individual polynomial background for each color channel. Dashed vertical lines mark the Descartes angles for the tertiary rainbow. The data were read out at 0.01° intervals of angular distance and have subsequently been smoothed by a moving average of 0.4° width [solid lines in (b)]. While barely visible in (a), each curve shows a pronounced maximum in (b). These maxima are observed at 41.1° (red), 39.9° (green), and 38.5° (blue) distance from the Sun, respectively. This corresponds to a shift of 0.4° − 0.8° in sunward direction with respect to their individual Descartes angles. This shift is in qualitative agreement with corrections obtained from wave optics.

of about 0.4°–0.5° in the sunward direction with respect to each Descartes angle [33]. However, the actual drop-size distribution during our observation is unknown. Simply transferring it from a fit to the simultaneously visible primary and secondary bows would be a questionable procedure since the tertiary bow is generated by drops located in a different part of the rain shower, thus possibly exhibiting different sizes. Because of these complications, we stayed with geometrical optics for our analysis.

Also, consequences of nonspherical raindrops for the tertiary rainbow have been discussed [34]. In case of a broad drop-size distribution containing a substantial amount of larger (and thus more oblate) drops, the tertiary might be wiped out with the exception of its lateral parts (approximately at the same elevation as the Sun, corresponding to a clock angle of zero). Consistent with this prediction, the bow fades into the zero-order glow background in our photo at higher clock angles in Fig. 2. For the visible segment itself, we can estimate contrast values of 1.1–1.5% from Figs. 6(a) and 6(b). However, we are aware that the photometric data are very likely influenced by additional aerosol and cloud background and thus not comparable to single drop simulations.

4. Outlook and Summary

Before concluding, we note that our advance notice of the natural tertiary rainbow has already stimulated an independent photographic proof of this bow in northern Germany only a month after our photo [35]. This second sighting appears to have been both brighter and longer-lived, which allowed several photographs of it to be taken. Subsequent stacking of these single frames (as known from ice-crystal halo research [36]) yielded a composite image averaging over raindrop fluctuations and sensor noise, in which both the tertiary and quaternary bow are clearly visible [37].

In summarizing, we have presented what we consider the first reliable photograph of the natural tertiary rainbow, as observed in southern Germany on May 15, 2011. To support our claim, a detailed calibration and analysis of the image was carried out in order to compare the recorded pattern with the predictions from geometric optics for spherical drops. We found a very satisfying agreement for both angular position and width of the bow. According to theory, the contrast of the phenomenon with respect to the zero-order glow background is very low, thus precluding unambiguous visual observation in most situations, with the possible exception of very rarely combined circumstances of favorable illumination, background, and the strength of rain. Consequently, photographs have to be taken without seeing the object of interest, and need strong processing. Nonetheless, due to the high interest and numerous rumors about the tertiary rainbow, we are convinced that this work marks a substantial progress in the field of atmospheric optics.

References and Notes

1. J. A. Adam, "The mathematical physics of rainbows and glories," Phys. Rep. **356**, 229–365 (2002).
2. R. L. Lee, Jr., "Mie theory, Airy theory, and the natural rainbow," Appl. Opt. **37**, 1506–1519 (1998).
3. A. B. Fraser, "Why can the supernumerary bows be seen in a rain shower?" J. Opt. Soc. Am. **73**, 1626–1628 (1983).
4. Y. Ayatsuka, "Ungewöhnliche Regenbögen," Meteoros **9**, 128–136 (2006).
5. L. Cowley, "Twinned rainbows," http://www.atoptics.co.uk/rainbows/twin1.htm.
6. L. Cowley, "Reflection rainbows," http://www.atoptics.co.uk/rainbows/reflect.htm.
7. R. Greenler, *Rainbows, Halos, and Glories* (Cambridge, 1980), pp. 6–7.
8. J. A. Adam, "The mathematical physics of rainbows and glories," Phys. Rep. **356**, 229–365 (2002), see in particular p. 243.
9. Named after a hypothetical zero-order rainbow, i.e., a rainbow without any internal reflection. This possibility has caused some rumors in history. However, due to the monotonic character of the deflection function of zero-order scattering, a zero-order rainbow does not exist [12]. Nonetheless in the Sun facing hemisphere, zero-order scattered light is dominating.
10. R. L. Lee, Jr. and P. Laven, "Visibility of natural tertiary rainbows," Appl. Opt. **50**, F152–F161.
11. This estimation is somehow difficult because of the intensity singularity at the angle of extreme deviation for the tertiary rainbow. Such singularities are typical features for caustics within geometric optics calculations.
12. P. Laven, 9 Russells Crescent, Horley, Surrey, RH6 7DJ, United Kingdom (personal communication, 2011).
13. C. B. Boyer, "The tertiary rainbow: An historical account," ISIS (1913-) / Isis **49**, 141–154 (1958).
14. T. C. Lewis, "A tertiary rainbow," Nature **32**, 523–626 (1885).
15. W. R. Corliss, *Rare Halos, Mirages, Anomalous Rainbows and Related Electromagnetic Phenomena* (1984), pp. 30–31.
16. R. L. Lee, Jr. and A. B. Fraser, *The Rainbow Bridge: Rainbows in Art, Myth, and Science* (Bellingham, 2001), pp. 290–295.
17. D. E. Pedgley, "A tertiary rainbow," Weather **41**, 401 (1986).
18. J. D. Walker, "Multiple rainbows from single drops of water and other liquids," Am. J. Phys. **44**, 421–432 (1976).
19. F. Billet, "Mémoirs sur les dix-neuf premiers arcs-en-ciel de l'eau," Annales Scientifiques de l'Ecole Normale Supérieure **5**, 67–109(1868).
20. R. L. Lee, Jr. and P. Laven, "Visibility of natural tertiary rainbows," Appl. Opt. **50**, F152–F161.
21. Arbeitskreis Meteore e.V. http://www.meteoros.de/indexe.htm.
22. M. Großmann, "Regenbogen 3. Ordnung 15.05.2011," http://www.meteoros.de/php/viewtopic.php?t=8463.
23. M. Großmann, "Natural tertiary rainbow 3rd order," http://atoptics.wordpress.com/2011/06/01/rainbow-3th-order-3/.
24. as quoted from [17] by Cowley in http://www.atoptics.co.uk/rainbows/ord34.htm.
25. Our method is based on the well-known transformation routines from one angular coordinate system into another, e.g., from declination and right ascension into elevation and azimuth for astronomical purposes. Here, we have to deal with four such coordinate systems, having their individual poles at (1) the center of the star field image, (2) the zenith, (3) the center of the rainbow image, and (4) the Sun.
26. A. Haußmann, "Die rechnerische Bestimmung von Winkeldistanzen und Positionen durch die Vermessung von Fotos," http://www.meteoros.de/download/haussmann/NLC-Haussmann.zip.
27. W. Tape and J. Moilanen, *Atmospheric Halos and the Search for Angle x* (American Geophysical Union, 2005), pp. 203–210.

28. C. Mauer, "Measurement of the spectral response of digital cameras with a set of interference filters," Diploma thesis (University of Applied Sciences Cologne, 2009).
29. M. Menat, "Atmospheric phenomena before and during sunset," Appl. Opt. **19**, 3458–3468 (1980).
30. International Association for the Properties of Water and Steam, "Release on the refractive index of ordinary water substance as a function of wavelength, temperature and pressure," (1997), http://www.iapws.org/relguide/rindex .pdf.
31. J. A. Adam, "The mathematical physics of rainbows and glories," Phys. Rep. **356**, 229–365 (2002), see in particular pp. 243–245.
32. R. L. Lee, Jr. and P. Laven, "Visibility of natural tertiary rainbows," Appl. Opt. **50**, F152–F161.
33. P. Laven, "Mieplot Software," http://www.philiplaven.com/ mieplot.htm.
34. D. S. Langley and P. L. Marston, "Generalized tertiary rainbow of slightly oblate drops: observations with laser illumination," Appl. Opt. **37**, 1520–1526 (1998).
35. M. Theusner, "3rd and 4th order rainbows," http://atoptics .wordpress.com/2011/06/12/3rd-and-4th-order-rainbows/.
36. W. Tape and J. Moilanen, *Atmospheric Halos and the Search for Angle x* (American Geophysical Union, 2005), pp. 200–201.
37. M. Theusner, "Photographic observation of a natural fourth-order rainbow," Appl. Opt. **50**, F129–F133.